STRUCTURAL CHEMISTRY

ISSN 2053-2296

Crystallization of metastable monoclinic carnallite, $KCl{\cdot}MgCl_2{\cdot}6H_2O$: missing structural link in the carnallite family

Melanie Pannach, Iris Paschke, Horst Schmidt, Daniela Freyer* and Wolfgang Voigt*

Institut für Anorganische Chemie, TU Bergakademie Freiberg, Leipziger Strasse 29, Freiberg 09599, Germany. *Correspondence e-mail: daniela.freyer@chemie.tu-freiberg.de, wolfgang.voigt@chemie.tu-freiberg.de

Received 19 February 2020
Accepted 13 April 2020

Edited by H. Uekusa, Tokyo Institute of Technology, Japan

Keywords: crystallization; metastable; monoclinic; potassium carnallite; crystal structure; potash; fertilizer.

CCDC reference: 1984700

Supporting information: this article has supporting information at journals.iucr.org/c

During evaporation of natural and synthetic K–Mg–Cl brines, the formation of almost square plate-like crystals of potassium carnallite (potassium chloride magnesium dichloride hexahydrate) was observed. A single-crystal structure analysis revealed a monoclinic cell [a = 9.251 (2), b = 9.516 (2), c = 13.217 (4) Å, β = 90.06 (2)° and space group $C2/c$]. The structure is isomorphous with other carnallite-type compounds, such as $NH_4Cl{\cdot}MgCl_2{\cdot}6H_2O$. Until now, natural and synthetic carnallite, $KCl{\cdot}MgCl_2{\cdot}6H_2O$, was only known in its orthorhombic form [a = 16.0780 (3), b = 22.3850 (5), c = 9.5422 (2) Å and space group $Pnna$].

1. Introduction

The natural evaporitic mineral carnallite, $KCl{\cdot}MgCl_2{\cdot}6H_2O$, is a main source for potash fertilizer production and for the production of magnesium chloride. Double salts with the general formula $MX{\cdot}M'X_2{\cdot}6H_2O$, where M is a large monovalent cation, M' is a small divalent cation and X is Cl^-, Br^- or I^-, represent a family of structurally similar compounds. With the exception of $M = K^+$ or $Li(H_2O)^+$, carnallite-type compounds crystallize with a monoclinic lattice (see Table 1). As can be seen in Table 1, the monoclinic angle for all compounds is near 90° and the respective basis plane is nearly square. Therefore, in older references, the cell was described as 'tetragonal' and 'weak monoclinic' (Andress & Saffe, 1939).

The structures of carnallites are typically described as perovskite-like, with the halide anions arranged octahedrally around the monovalent cations. The corners of these octahedra are linked to neighbouring octahedra, forming a cubic lattice with large holes having cuboctahedron geometry. The cations inside the cuboctahedron have contact with 12 nearest equidistant anions. In the case of the carnallites, these are the divalent hydrated M' cations. Thus, the six water molecules of M' can form 12 hydrogen bonds with the halide anions. Small distortions lower the symmetry of the lattice (in the case of monoclinic carnallites), while the general arrangement of atoms remains.

An alternative description of the perovskite lattice is a cubic close-packed stacking of anions with cations (here M) occupying the octahedral holes. This is valid for all known carnallite-type structures, except for the mineral carnallite itself, where every third layer consists of a hexagonal stack denoted as *hcc*. The unit cell is enlarged to six layers, symbolized as a 6H structure. A hexagonal stack means the adjacent octahedra share faces. In this way, the mineral carnallite represents an exception to all other double salts of this stoichiometry.

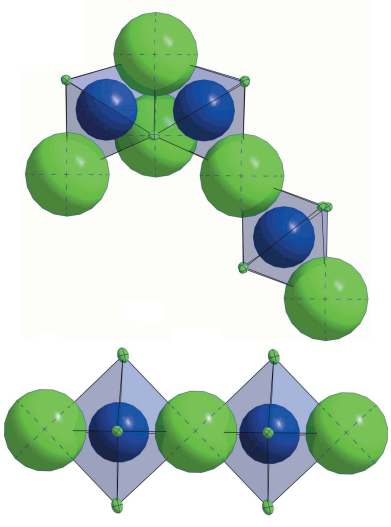

Table 1
Survey of the crystallographic data of carnallite-type double salts.

Formula	Space group	Cell axes (Å)			β	Z	X-ray[a]	Reference
$[Li(H_2O)][Mg(H_2O)_6]Cl_3$	$C2/m$	9.2	9.7	13.4	93.3		P	Emons *et al.* (1988)
	$R3$	9.2		12.0		3	SC	Schmidt *et al.* (2009)
$K[Mg(H_2O)_6]Cl_3$	$Pbnn$	9.6	16.0	22.6				Leonhardt (1930)
	$Pban$	9.5	16.0	22.5		12	SC	Andress & Saffe (1939)
	$Pnna$	9.6	16.1	22.6			SC	Fischer (1973)
	$Pnna$	16.1	22.5	9.5		12	SC	Schlemper *et al.* (1985)
$Rb[Mg(H_2O)_6]Cl_3$	$P4/n$	13.3	6.6	6.6		2	SC	Andress & Saffe (1939)
	$C2/c$	9.3	9.5	13.3	90.2	4	SC[b]	Marsh (1992*a*)
	$C2/c$	9.3	9.6	13.3	90.4		P	Emons *et al.* (1988)
$(NH_4)[Mg(H_2O)_6]Cl_3$	$P4/n$	13.3	6.7	6.7		2	SC	Andress & Saffe (1939)
	$C2/c$	9.3	9.6	13.3	90.1	4	SC	Solans *et al.* (1983)
	$C2/c$	9.3	9.5	13.3	90.1	4	SC[b]	Marsh (1992*b*)
$Cs[Mg(H_2O)_6]Cl_3$	$C2/c$	9.4	9.6	13.3	90.3		P	Emons *et al.* (1988)
$K[Mg(H_2O)_6]Br_3$	$P4/n$	13.6	6.8	6.8			SC	Andress & Saffe (1939)
$Rb[Mg(H_2O)_6]Br_3$	$C2/c$	9.6	9.8	13.8	90.1		P	Emons *et al.* (1988)
	$C2/c$	9.6	9.9	13.8	90.1	4	P	Dinnebier *et al.* (2008)
$T \geq 85$ °C	$Pm\bar{3}m$	6.94	6.94	6.94		1	P	Dinnebier *et al.* (2008)
$(NH_4)[Mg(H_2O)_6]Br_3$	$C2/c$	9.6	9.8	13.7	90.2		P	Emons *et al.* (1988)
$Cs[Mg(H_2O)_6]Br_3$	$C2/c$	9.8	9.9	13.9	90.1		P	Emons *et al.* (1988)
	$C2/c$	9.8	10.0	14.0	90.1	4	P	Dinnebier *et al.* (2008)
$K[Mg(H_2O)_6]I_3$	$C2/c$	10.0	10.2	14.4	90.1		P	Emons *et al.* (1988)
$Rb[Mg(H_2O)_6]I_3$	$C2/c$	10.0	10.3	14.5	90.6		P	Emons *et al.* (1988)
$(NH_4)[Mg(H_2O)_6]I_3$	$C2/c$	10.0	10.2	14.3	90.4		P	Emons *et al.* (1988)
$Cs[Mg(H_2O)_6]I_3$	Compound not known							
$(NH_4)[Fe(H_2O)_6]Br_3$	Synthesis only							Mercier (1937)
$K[Ni(H_2O)_6]Br_3$	$C2/c$	9.5	9.7	13.6	90.1	4	SC	Tepavitcharova *et al.* (1997)
$(NH_4)[Ni(H_2O)_6]Br_3$	$C2/c$	9.6	9.8	13.7	90.2	4	SC	Tepavitcharova *et al.* (1997)
$Rb[Co(H_2O)_6]Br_3$	$C2/c$	9.6	9.8	13.7	90.1	4	SC	Tepavitcharova *et al.* (1997)
$(NMe_4)[Mg(H_2O)_6]Br_3$	$P2_12_12_1$	7.7	9.4	22.5			SC	Gusev *et al.* (2011)
Mixed crystals								
$(NH_4)_xK_{(1-x)}[Mg(H_2O)_6]Cl_3$								
$x = 0.33$							P	Siemann (1994)
$x = 0.36$	$P2/c$ or Pc	6.7	6.7	13.2	90			Herbert *et al.* (1995)
$x = 0.5$	$C2/c$	9.3	9.5	13.2	90.2	4	SC	Okrugin *et al.* (2019)
$x = 0.52$		9.3	9.6	13.3	90.1		SC	Yang *et al.* (2019)
$K[Mg(H_2O)_6][Br_xCl_{(1-x)}]_3$								
$0 < x < 0.12$	Rhombic–pseudohexagonal						SC	Andress & Saffe (1939)
$0.12 < x < 0.85$	Tetragonal						SC	Andress & Saffe (1939)
$0.85 < x < 1.0$	Rhombic–pseudotetragonal						SC	Andress & Saffe (1939)

Notes: (*a*) P = powder XRD and SC = single-crystal XRD; (*b*) recalculated from the triclinic cells given by Waizumi *et al.* (1991).

Emons *et al.* (1988) applied the concept of a 'tolerance factor, t', known from oxidic perovskites ABO_3 (Wells, 1984) to the carnallite-type. With

$$t = \frac{r_A + r_O}{\sqrt{2} \cdot (r_B + r_O)}$$

and setting $r_A = r_{M'}$, $r_B = r_M$ and $r_O = r_X$, the authors showed that with reasonable values of the radii, the factor t should not exceed values of about 1.045 to 1.061. The values obtained for $KBr{\cdot}MgBr_2{\cdot}6H_2O$ and $KCl{\cdot}MgCl_2{\cdot}6H_2O$ are 1.045 and 1.061, respectively. The bromide salt is monoclinic and the chloride exhibits a hexagonal stack with a threefold larger orthorhombic unit cell. Thus, the combination of potassium and magnesium with chloride is at the border of stability of pure cubic close packing. In the case of the smaller sodium ion, a much larger value is obtained, which explains why this type of double salt with sodium does not exist.

The K–Mg–Cl carnallite can form mixed crystals with corresponding (NH$_4$)–Mg–Cl and K–Mg–Br double salts. Already at relatively small amounts of ammonium or bromide, the structure changes from orthorhombic to monoclinic.

Thermoanalytical investigations revealed solid-solid phase transitions for $(NH_4)Br{\cdot}MgBr_2{\cdot}6H_2O$, $RbBr{\cdot}MgBr_2{\cdot}6H_2O$ (Emons *et al.*, 1991) and $CsCl{\cdot}MgCl_2{\cdot}6H_2O$ (Emons *et al.*, 1987). An endothermic effect at 435 K for $RbBr{\cdot}MgBr_2{\cdot}6H_2O$ was suggested to be caused by an impurity of $MgBr_2{\cdot}6H_2O$ (Emons *et al.*, 1991). Dinnebier *et al.* (2008) recorded temperature-dependent powder X-ray diffraction patterns, showing that $RbBr{\cdot}MgBr_2{\cdot}6H_2O$ undergoes a reversible transition to a cubic perovskite structure, where the $[Mg(H_2O)_6]$ octahedron is fourfold disordered. The temperature dependence of the lattice parameters of the analogous caesium compound showed a kink at around 430 K, but no symmetry break, which is in agreement with the absence of a thermal effect. Later, the same authors described the powder pattern of the high-temperature form of $RbBr{\cdot}MgBr_2{\cdot}6H_2O$ by means of a rigid-body rotation of the $[Mg(H_2O)_6]$ octahedra.

A survey on hydrated double salts $MX{\cdot}M'X_2{\cdot}n\mathrm{H_2O}$ (M = K^+, NH_4^+, Rb^+ or Cs^+; M' = Mg^{2+}, Mn^{2+}, Fe^{2+}, Co^{2+}, Ni^{2+} or Cu^{2+}; X = Cl^-, Br^- or I^-) was given by Balarew & Tepavitcharova (2003). The authors discussed the solid phase structure and coordination in relation to the complexes and the concentration expected in saturated solutions.

The reason for the present investigation was the observation of a particular crystallization behaviour in brine samples from an underground nuclear repository in Morsleben (Niedersachsen, Germany). The brines were nearly saturated with carnallite, but during evaporation in laboratory dishes at room temperature, instead of the expected typical pseudo-hexagons of carnallite mineral, crystals of prismatic, nearly cubic, morphology were observed. In the same mine, Siemann (1994) and Herbert *et al.* (1995) discovered ammonium-bearing carnallite with a monoclinic lattice. However, preliminary investigations regarding brine composition by ion chromatography excluded the presence of ammonium in the brine; furthermore, no bromide was found in the crystal. Selection of a single crystal and performance of a preliminary lattice determination suggested the presence of a new phase.

2. Experimental

2.1. Synthesis and crystallization

To reproduce the crystallization of the unknown phase from natural brine, a series of pure synthetic solutions (4.1 molal $MgCl_2$ + 0.2 molal KCl/4.7 molal $MgCl_2$ + 0.05 molal KCl) were prepared and evaporated slowly over a period of 2–4 d in quiescent crystallization dishes (about 5 ml) at room temperature. Since it was speculated that impurities could influence nucleation, the addition of bromide (0.0025 to 0.01 molal) and sulfate (0.01 to 0.04 molal) was used to simulate the impurities of the natural Morsleben mine samples. Two samples were not spiked with bromide or sulfate. While sulfate will not be incorporated into the solid phase, bromide is expected to form a solid solution with the chloride in the carnallite. However, the distribution coefficient of bromide between carnallite and its solution in mass% has a value of about 0.5 (Braitsch, 1962), which with an impurity level of 0.01 mol kg^{-1} H_2O (0.6 mass% Br^-) yields a maximum content of 0.3 mass% Br^- in the carnallite. The latter corresponds to about 0.15 mol% Br^- in the carnallite. Nine evaporation experiments (starting solution compositions are listed in Table 2) were performed, confirming the observation that the plate-like nearly square (monoclinic) morphology appears first or simultaneously with the pseudo-hexagonal carnallite. This was true for all solutions, both the spiked and unspiked. After some hours, the monoclinic form dissolves and the known pseudo-hexagonal form remains (see photographs in Fig. 1). Podder *et al.* (2013) also observed 'quadratic plates' in their experiments to grow carnallite crystals; however, they hypothesized the presence of a type of surface-grown 'Hopper crystals'. Contrary to Podder *et al.*, we also observed the growth of square crystals on the bottom of the dishes. Thus, surface-influenced nucleation cannot be considered as crucial to obtain the monoclinic form of carnallite.

Table 2
Initial solution compositions (m in mol kg^{-1} H_2O) of the nine evaporation experiments.

No.	$m(Mg^{2+})$	$m(K^+)$	$m(Cl^-)$	$m(SO_4^{2-})$	$m(Br^-)$
1	4.086	0.192	8.300	0	0
2	4.630	0.050	9.326	0	0
3	4.70	0.054	9.45	0	0.0028
4	4.70	0.057	9.45	0	0.0055
5	4.70	0.059	9.45	0	0.0074
6	4.70	0.062	9.45	0	0.0106
7	4.725	0.069	9.509	0.011	0
8	4.753	0.089	9.451	0,.21	0
9	4.735	0.108	9.32	0.030	0

2.2. Single-crystal analysis and refinement

Crystal data, data collection and structure refinement details are summarized in Table 3. For single-crystal diffraction with a Stoe IPDS II image-plate diffraction system, a suitable crystal was selected under the microscope in polarized

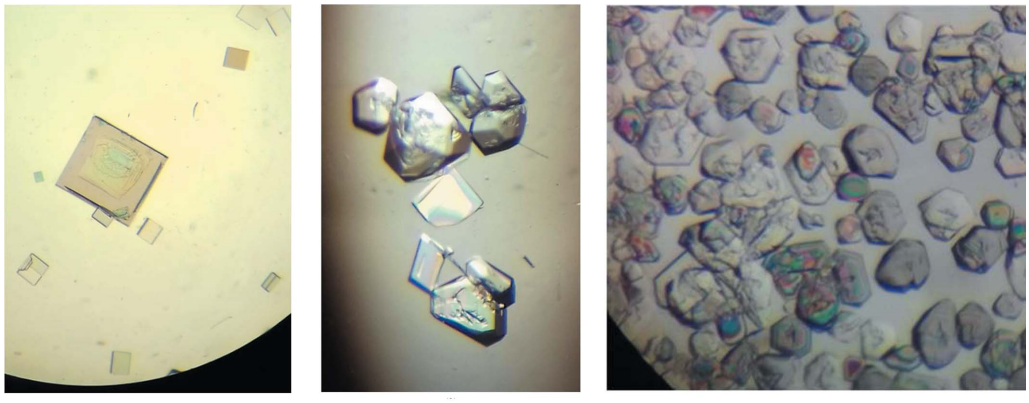

Figure 1
Microscope photos of monoclinic crystals (left), along with the pseudo-hexagonal carnallite crystallites formed over time (middle). Eventually, monoclinic $KCl{\cdot}MgCl_2{\cdot}6H_2O$ dissolves completely and the well-known pseudo-hexagonal forms remain (right). Crystallite edge lengths are on average between 0.1 and 0.5 mm.

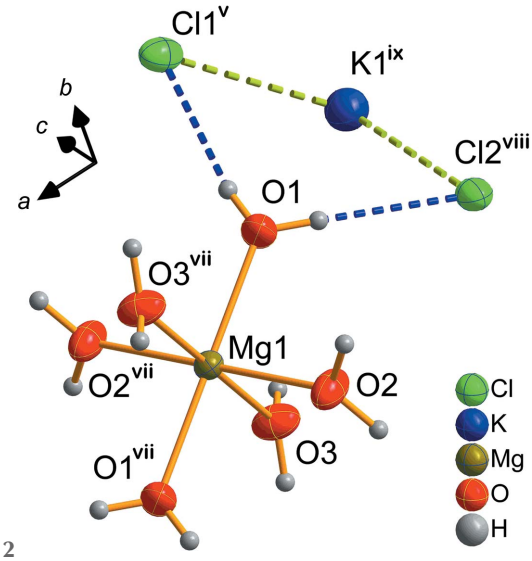

Figure 2
The asymmetric unit and symmetry-related atoms of $KCl{\cdot}MgCl_2{\cdot}6H_2O$. Displacement ellipsoids are drawn at the 50% probability level and H atoms are not labelled. [Symmetry codes: (v) $x+\frac{1}{2}, -y+\frac{3}{2}, z+\frac{1}{2}$; (vii) $-x+2, -y+1, -z+1$; (viii) $-x+\frac{1}{2}, y-\frac{1}{2}, -z+\frac{1}{2}$; (ix) $-x+\frac{1}{2}, -y+\frac{3}{2}, -z+1$.]

light. The crystal was fixed by high-purity silicon grease on a 0.1 mm diameter Hilgenberg glass capillary and after determination of the monoclinic unit cell, a triclinic strategy based on this cell was applied for the measurement of the diffracted intensities at a temperature of 200 K.

A structure solution using direct methods and a refinement of the atomic positions led to the atomic coordinates of the K, Mg, O and Cl ions. The positions of the H atoms could be located from residual electron-density maxima after further refinement. Anisotropic displacement parameters were determined for the heavy atoms and refinement of isotropic displacement parameters was performed for H atoms.

Further analysis showed that there was a continuous drop in intensity during the measurement period, indicating the beginning of crystal decomposition. The drop in intensity was taken into account by applying a decay correction. Thus, the R_{int} value was reduced from 8.00 to 4.58%.

An attempt to perform chemical analysis on single crystallites using SEM–EDX (scanning electron microscopy with energy dispersive X-ray analysis) did not lead to a representative result, as the adherent mother liquor could not be completely removed. Hence, slightly higher magnesium and chloride contents were always measured in comparison to potassium. However, structure analysis revealed an unambiguous K:Mg:Cl ratio of 1:1:3 in the crystal, which crystallized from a solution containing only KCl and $MgCl_2$ (No. 2 in Table 2).

3. Results and discussion

Contrary to orthorhombic carnallite, the structure of the new monoclinic form of $KCl{\cdot}MgCl_2{\cdot}6H_2O$ contains only one crystallographic position for Mg and one for K, as shown in Fig. 2.

Table 3
Experimental details.

Crystal data	
Chemical formula	$KCl{\cdot}MgCl_2{\cdot}6H_2O$
M_r	277.86
Crystal system, space group	Monoclinic, *C*2/*c*
Temperature (K)	200
a, *b*, *c* (Å)	9.251 (2), 9.516 (2), 13.217 (4)
β (°)	90.06 (2)
V (Å^3)	1163.6 (5)
Z	4
Radiation type	Mo $K\alpha$
μ (mm^{-1})	1.19
Crystal size (mm)	0.3 × 0.26 × 0.06
Data collection	
Diffractometer	Stoe IPDS 2T
Absorption correction	Integration Coppens (1970)
T_{min}, T_{max}	0.665, 0.983
No. of measured, independent and observed [$I > 2\sigma(I)$] reflections	6028, 1341, 1096
R_{int}	0.046
(sin $\theta/\lambda)_{max}$ (Å^{-1})	0.650
Refinement	
$R[F^2 > 2\sigma(F^2)]$, $wR(F^2)$, *S*	0.035, 0.096, 1.21
No. of reflections	1341
No. of parameters	78
H-atom treatment	All H-atom parameters refined
$\Delta\rho_{max}$, $\Delta\rho_{min}$ (e Å^{-3})	0.25, −0.49

Computer programs: *X-AREA* (Stoe & Cie, 2002), *X-RED32* (Stoe & Cie, 2002), *SHELXT* (Sheldrick, 2015*a*), *SHELXL2016* (Sheldrick, 2015*b*) and *DIAMOND* (Brandenburg, 2017).

The structure, which is isotypic with all other monoclinic carnallite-type double salts, displays a distorted perovskite-like lattice with corner-linked KCl_6 octahedra and single $Mg(H_2O)_6$ octahedra in its large 12-fold coordinated holes.

In Fig. 3, the unit cells of orthorhombic and monoclinic carnallite are compared. In the orthorhombic structure, two thirds of the KCl_6 octahedra are face-linked, resulting in a 6H unit cell. Fig. 4 emphasizes this coordination for potassium and chloride ions.

While packing considerations between cations and anions are important for structure formation, the strengths of hydrogen bonds (bond lengths and angles) should also have a significant effect. Table 4 lists the hydrogen bonds with bond lengths between 2.28 (4) and 2.44 (3) Å. However, the energetic balance between the various types of interactions are delicate. There is no easy argument for a decision regarding the predominant effect. For example, one should expect larger bond distances in the metastable monoclinic form in comparison to the stable orthorhombic form; however, adding all H···Cl hydrogen-bond lengths from the water molecules of the two crystallographically distant $Mg(H_2O)_6$ octahedra in the orthorhombic structure yields a value of 57.44 Å, whereas double the same distance for Mg1 in the monoclinic structure gives 56.28 Å. The mean Mg—O distances in the orthorhombic and monoclinic structures are 2.044 and 2.047 Å, respectively.

The observation that the monoclinic form dissolves after some time proves its metastability. Metastable phases should possess lower densities than the stable forms. Our calculated density at 200 K is 1.586 Mg m^{-3}, while Schlemper *et al.* (1985)

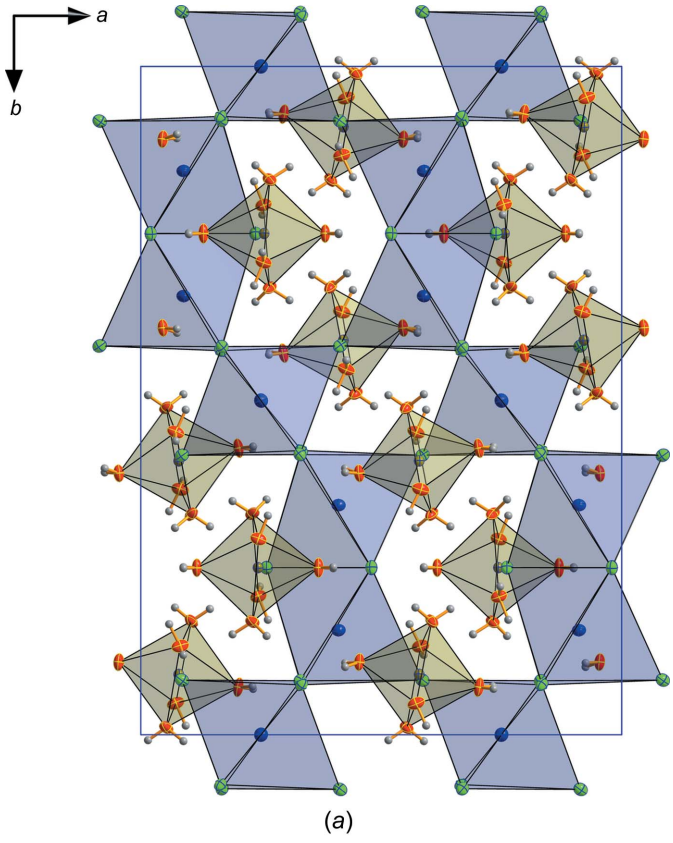

Figure 3
Comparison of the unit cells of (*a*) orthorhombic and (*b*) monoclinic $KCl{\cdot}MgCl_2{\cdot}6H_2O$.

Table 4
Hydrogen-bond geometry (Å, °).

D—H···*A*	*D*—H	H···*A*	*D*···*A*	*D*—H···*A*
O3—H3*B*···Cl2^{i}	0.81 (3)	2.34 (3)	3.1345 (18)	172 (3)
O3—H3*A*···Cl1^{ii}	0.82 (3)	2.36 (3)	3.1703 (19)	167 (3)
O2—H2*B*···Cl1^{iii}	0.89 (4)	2.31 (4)	3.1689 (18)	164 (3)
O2—H2*A*···Cl1^{iv}	0.86 (4)	2.28 (4)	3.1369 (18)	172 (3)
O1—H1*B*···Cl1^{v}	0.81 (4)	2.35 (4)	3.1500 (18)	171 (4)
O1—H1*A*···Cl2^{vi}	0.75 (3)	2.44 (3)	3.1863 (19)	171 (3)

Symmetry codes: (i) $-x+1, y-1, -z+\frac{1}{2}$; (ii) $-x+1, -y+1, -z+1$; (iii) $-x+1, y, -z+\frac{1}{2}$; (iv) $x+\frac{1}{2}, y-\frac{1}{2}, z$; (v) $x+\frac{1}{2}, -y+\frac{3}{2}, z+\frac{1}{2}$; (vi) $-x+\frac{1}{2}, y-\frac{1}{2}, -z+\frac{1}{2}$.

calculated a value of 1.60 Mg m^{-3} at room temperature for the orthorhombic form. The experimental density determination of Andress & Saffe (1939) gave a value of 1.602 Mg m^{-3}. Thus, our density value (even if only slightly lower) confirms the metastability of monoclinic $KCl{\cdot}MgCl_2{\cdot}6H_2O$. The small density difference cannot be easily recognized when comparing some selected bond lengths.

With regard to the faster crystallization of the metastable phase (Ostwald's step rule), the variability of the $Mg(H_2O)_6$ octahedra in the two carnallite structures also provides a possible explanation. All O—Mg—O angles in the metastable monoclinic structure are very close to 90° [between 89.90 (7) and 90.10 (7)°], while in the orthorhombic structure, according to the data of Schemper *et al.*, the $Mg(H_2O)_6$ octahedra are more distorted (89.46–94.83° for Mg1 and 88.71–91.48° for Mg2). Undistorted $Mg(H_2O)_6$ octahedra, as they exist in solution, are incorporated more quickly into a crystal lattice with only minimal changes. For the formation of more

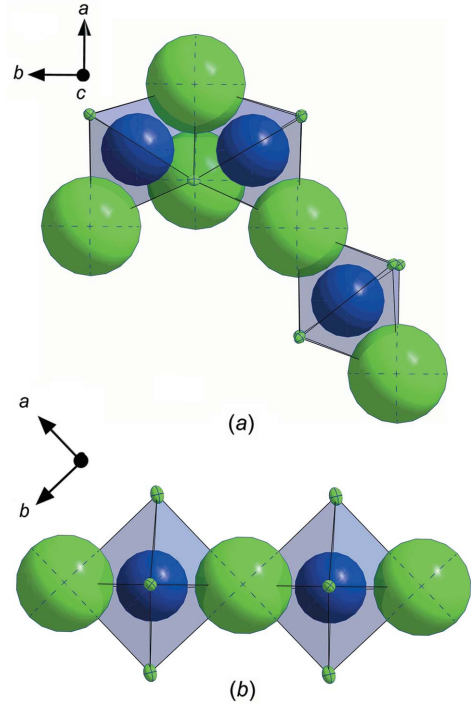

Figure 4
Comparison of the K–Cl octahedra and their connectivity in (*a*) orthorhombic and (*b*) monoclinic $KCl{\cdot}MgCl_2{\cdot}6H_2O$. Colour key: K blue and Cl green.

distorted geometries, even with an energetically balanced arrangement over the whole lattice, longer crystallization times are required.

4. Conclusion

Crystallization experiments with natural and synthetic potash salt brines revealed the formation of a new phase of potassium carnallite, *i.e.* $KCl{\cdot}MgCl_2{\cdot}6H_2O$. Crystal structure analysis yielded a monoclinic form of potassium carnallite, for which the crystal structure was solved. The monoclinic form represents the stable form of all other members of the carnallite family (except lithium carnallite), but was missing for potassium carnallite until now. The radii of K^+, $[Mg(H_2O)_6]^{2+}$ and Cl^- in $KCl{\cdot}MgCl_2{\cdot}6H_2O$ are in the border region of stability for the simple cubic close-packed anion stacking similar to a perovskite lattice. However, nucleation and growth of the 'normal' monoclinic potassium carnallite can be observed in brines. The phase is metastable and transforms *via* a dissolution–crystallization mechanism into the stable orthorhombic form after some time. Since the nucleation and crystallization kinetics represent an important issue in industrial crystallization, future investigation of the kinetics should consider the possible formation of monoclinic carnallite.

Acknowledgements

We would like to thank the unknown referees for hints, which have led to an improved evaluation of the measured diffraction data, as well as to a further explanation of the metastable occurrence of carnallite.

References

Andress, K. R. & Saffe, A. (1939). *Z. Kristallogr.* **101**, 1–6.
Balarew, C. & Tepavitcharova, S. (2003). *Monatsh. Chem.* **134**, 721–734.
Braitsch, O. (1962). *Entstehung und Stoffbestand der Salzlagerstätten*, in *Mineralogie und Petrographie in Einzeldarstellungen*, edited by W. V. Engelhardt & J. Zemann. Berlin, Göttingen, Heidelberg: Springer-Verlag.
Brandenburg, K. (2017). *DIAMOND*. Crystal Impact GbR, Bonn, Germany.
Coppens, P. (1970). *Crystallographic Computing*, edited by F. R. Ahmed, S. R. Hall & C. P. Huber, pp. 255–270. Copenhagen: Munksgaard.
Dinnebier, R. E., Liebold-Ribeiro, Y. & Jansen, M. (2008). *Z. Anorg. Allg. Chem.* **634**, 1857–1862.
Emons, H.-H., Brand, P., Pohl, T. & Köhnke, K. (1988). *Z. Anorg. Allg. Chem.* **563**, 180–184.
Emons, H.-H., Voigt, H., Naumann, R. & Pohl, T. (1991). *J. Therm. Anal.* **37**, 1605–1619.
Emons, H.-H., Voigt, H., Pohl, T. & Naumann, R. (1987). *Thermochim. Acta*, **121**, 151–163.
Fischer, W. (1973). *N. Jb. Miner. Mh.* **3**, 100–109.
Gusev, I. M., Skripkin, Yu. M., Spektor, K. K. & Starova, G. L. (2011). *Russ. J. Gen. Chem.* **81**, 623–627.
Herbert, H.-J., Sander, W., Blanke, H., Baitz, S., Jacobi, H. & Follner, H. (1995). *N. Jb. Miner. Mh.* **8**, 351–358.
Leonhardt, J. (1930). *Kali*, **24**, 277–282.
Marsh, R. E. (1992*a*). *Acta Cryst.* C**48**, 218–219.
Marsh, R. E. (1992*b*). *Acta Cryst.* C**48**, 972.
Mercier, J.-M. (1937). *Compt. Rend. Chim.* **204**, 500–502.
Okrugin, V., Kudaeva, S., Karimova, O., Yakubovich, O., Belakovskiy, D., Chukanov, N., Zolotarev, A., Gurzhiy, V., Zinovieva, N., Shiryaev, A. & Kartashov, P. (2019). *MinMag*, **83**, 223–231.
Podder, J., Gao, S., Evitts, R. W., Besant, R. W. & Matthews, W. (2013). *J. Metals Mater. Miner.* **23**(2), 37–41.
Schlemper, E. O., Sen Gupta, P. K. & Zoltai, T. (1985). *Am Mineral.* **70**, 1309–1313.
Schmidt, H., Euler, B., Voigt, W. & Heide, G. (2009). *Acta Cryst.* C**65**, i57–i59.
Sheldrick, G. M. (2015*a*). *Acta Cryst.* A**71**, 3–8.
Sheldrick, G. M. (2015*b*). *Acta Cryst.* C**71**, 3–8.
Siemann, M. G. (1994). *N. Jb. Miner. Mh.* **3**, 97–100.
Solans, X., Font-Altaba, M., Aguiló, M., Solans, J. & Domenech, V. (1983). *Acta Cryst.* C**39**, 1488–1490.
Stoe & Cie (2002). *X-AREA* and *X-RED32*. Stoe & Cie, Darmstadt, Germany.
Tepavitcharova, S., Macicek, J., Balarew, C., Tzvetkova, C. & Angelova, O. (1997). *J. Solid State Chem.* **129**, 200–205.
Waizumi, K., Masuda, H. & Ohtaki, H. (1991). *Am. Mineral.* **76**, 1884–1888.
Wells, A. F. (1984). *Structural Inorganic Chemistry*, 5th ed., p. 586. Oxford Science Publishers.
Yang, H., Chen, Y., Wang, M. & Li, B. (2019). *Crystallogr. Rep.* **64**, 277–281.

supporting information

Acta Cryst. (2020). C**76**, 507-512 [https://doi.org/10.1107/S2053229620005197]

Crystallization of metastable monoclinic carnallite, $KCl·MgCl_2·6H_2O$: missing structural link in the carnallite family

Melanie Pannach, Iris Paschke, Horst Schmidt, Daniela Freyer and Wolfgang Voigt

Computing details

Data collection: *X-AREA* (Stoe & Cie, 2002); cell refinement: *X-AREA* (Stoe & Cie, 2002); data reduction: *X-RED32* (Stoe & Cie, 2002); program(s) used to solve structure: SHELXT (Sheldrick, 2015a); program(s) used to refine structure: *SHELXL2016* (Sheldrick, 2015b); molecular graphics: **Please provide program name**; software used to prepare material for publication: *SHELXL2016* (Sheldrick, 2015b).

Potassium chloride magnesium dichloride hexahydrate

Crystal data

$KCl·MgCl_2·6H_2O$
M_r = 277.86
Monoclinic, *C*2/*c*
a = 9.251 (2) Å
b = 9.516 (2) Å
c = 13.217 (4) Å
β = 90.06 (2)°
V = 1163.6 (5) Å^3
Z = 4
F(000) = 568
D_x = 1.586 Mg m^{-3}
Mo *Kα* radiation, *λ* = 0.71073 Å
Cell parameters from 3875 reflections
θ = 3.1–27.4°
μ = 1.19 mm^{-1}
T = 200 K
Square planar crystals, colorless
0.3 × 0.26 × 0.06 mm

Data collection

Stoe IPDS 2T diffractometer
Radiation source: sealed X-ray tube, 12 x 0.4 mm long-fine focus
Plane graphite monochromator
Detector resolution: 6.67 pixels mm^{-1}
rotation method scans
Absorption correction: integration Coppens (1970)
T_{min} = 0.665, T_{max} = 0.983
1341 measured reflections
1341 independent reflections
1096 reflections with $I > 2\sigma(I)$
R_{int} = 0.046
θ_{max} = 27.5°, θ_{min} = 3.1°
h = −12→11
k = −12→12
l = −17→17

Refinement

Refinement on F^2
Least-squares matrix: full
$R[F^2 > 2\sigma(F^2)]$ = 0.035
$wR(F^2)$ = 0.096
S = 1.21
1341 reflections
78 parameters
0 restraints
Hydrogen site location: difference Fourier map
All H-atom parameters refined
$w = 1/[\sigma^2(F_o^2) + (0.0379P)^2 + 1.1854P]$ where $P = (F_o^2 + 2F_c^2)/3$
$(\Delta/\sigma)_{max} < 0.001$
$\Delta\rho_{max}$ = 0.25 e Å^{-3}
$\Delta\rho_{min}$ = −0.49 e Å^{-3}

Special details

Geometry. All esds (except the esd in the dihedral angle between two l.s. planes) are estimated using the full covariance matrix. The cell esds are taken into account individually in the estimation of esds in distances, angles and torsion angles; correlations between esds in cell parameters are only used when they are defined by crystal symmetry. An approximate (isotropic) treatment of cell esds is used for estimating esds involving l.s. planes.

Refinement. Further details of the crystal structure investigations may be obtained from the Fachinformationszentrum Karlsruhe, 76344 Eggenstein-Leopoldshafen, Germany (Fax: +49-7247-808-666; E-Mail: crysdata@fizkarlsruhe.de, http://www.fiz-karlsruhe.de/request for deposited data.html) on quoting the depository number CSD-1984700.

Fractional atomic coordinates and isotropic or equivalent isotropic displacement parameters (Å²)

	x	*y*	*z*	U_{iso}*/U_{eq}
Cl1	0.25176 (6)	0.73516 (6)	0.25262 (3)	0.03176 (18)
Cl2	0.000000	1.000000	0.000000	0.0309 (2)
K1	0.000000	0.99572 (8)	0.250000	0.0388 (2)
Mg1	1.000000	0.500000	0.500000	0.0183 (2)
O1	0.81961 (18)	0.60403 (19)	0.54985 (13)	0.0335 (4)
H1A	0.746 (4)	0.584 (4)	0.532 (2)	0.044 (8)*
H1B	0.812 (4)	0.648 (4)	0.602 (3)	0.068 (11)*
O2	0.9116 (2)	0.48620 (18)	0.35828 (12)	0.0336 (4)
H2A	0.875 (3)	0.412 (4)	0.331 (2)	0.052 (9)*
H2B	0.883 (3)	0.563 (4)	0.326 (2)	0.051 (9)*
O3	0.90679 (19)	0.31231 (17)	0.53761 (13)	0.0336 (4)
H3A	0.854 (3)	0.306 (3)	0.588 (2)	0.046 (8)*
H3B	0.937 (3)	0.235 (4)	0.524 (2)	0.045 (8)*

Atomic displacement parameters (Å²)

	U^{11}	U^{22}	U^{33}	U^{12}	U^{13}	U^{23}
Cl1	0.0418 (3)	0.0305 (3)	0.0230 (3)	−0.0097 (2)	0.0006 (2)	−0.00064 (17)
Cl2	0.0271 (4)	0.0242 (4)	0.0415 (4)	−0.0009 (2)	0.0001 (3)	0.0059 (3)
K1	0.0405 (4)	0.0393 (4)	0.0365 (4)	0.000	0.0008 (3)	0.000
Mg1	0.0200 (4)	0.0179 (4)	0.0168 (4)	−0.0002 (3)	0.0003 (3)	−0.0011 (3)
O1	0.0239 (8)	0.0403 (9)	0.0364 (9)	0.0042 (7)	−0.0002 (6)	−0.0144 (7)
O2	0.0491 (10)	0.0260 (8)	0.0256 (8)	0.0008 (7)	−0.0129 (7)	−0.0017 (6)
O3	0.0435 (10)	0.0201 (8)	0.0373 (9)	−0.0042 (6)	0.0146 (7)	−0.0009 (6)

Geometric parameters (Å, º)

Cl1—K1^{i}	3.2353 (10)	Mg1—O3	2.0450 (16)
Cl1—K1	3.4020 (10)	Mg1—O2	2.0473 (16)
Cl2—K1	3.3046 (9)	Mg1—O2^{iii}	2.0473 (16)
Cl2—K1^{ii}	3.3046 (9)	Mg1—O1	2.0497 (16)
Mg1—O3^{iii}	2.0450 (16)	Mg1—O1^{iii}	2.0497 (16)
K1^{i}—Cl1—K1	177.65 (2)	Cl1^{vi}—K1—Cl1	86.42 (3)
K1—Cl2—K1^{ii}	180.0	O3^{iii}—Mg1—O3	180.0
Cl1^{iv}—K1—Cl1^{v}	90.45 (3)	O3^{iii}—Mg1—O2	90.10 (7)
Cl1^{iv}—K1—Cl2^{vi}	90.16 (2)	O3—Mg1—O2	89.90 (7)

Cl1^{v}—K1—Cl2^{vi}	88.848 (19)	O3^{iii}—Mg1—O2^{iii}	89.90 (7)
Cl1^{iv}—K1—Cl2	88.848 (19)	O3—Mg1—O2^{iii}	90.10 (7)
Cl1^{v}—K1—Cl2	90.16 (2)	O2—Mg1—O2^{iii}	180.0
Cl2^{vi}—K1—Cl2	178.59 (3)	O3^{iii}—Mg1—O1	89.99 (7)
Cl1^{iv}—K1—Cl1^{vi}	177.65 (2)	O3—Mg1—O1	90.01 (7)
Cl1^{v}—K1—Cl1^{vi}	91.58 (2)	O2—Mg1—O1	90.04 (7)
Cl2^{vi}—K1—Cl1^{vi}	91.057 (19)	O2^{iii}—Mg1—O1	89.97 (7)
Cl2—K1—Cl1^{vi}	89.972 (19)	O3^{iii}—Mg1—O1^{iii}	90.01 (7)
Cl1^{iv}—K1—Cl1	91.58 (2)	O3—Mg1—O1^{iii}	89.99 (7)
Cl1^{v}—K1—Cl1	177.65 (2)	O2—Mg1—O1^{iii}	89.96 (7)
Cl2^{vi}—K1—Cl1	89.972 (19)	O2^{iii}—Mg1—O1^{iii}	90.04 (7)
Cl2—K1—Cl1	91.057 (19)	O1—Mg1—O1^{iii}	180.0

Symmetry codes: (i) $x+1/2, y-1/2, z$; (ii) $-x, -y+2, -z$; (iii) $-x+2, -y+1, -z+1$; (iv) $-x+1/2, y+1/2, -z+1/2$; (v) $x-1/2, y+1/2, z$; (vi) $-x, y, -z+1/2$.

Hydrogen-bond geometry (Å, º)

D—H···*A*	*D*—H	H···*A*	*D*···*A*	*D*—H···*A*
O3—H3*B*···Cl2^{vii}	0.81 (3)	2.34 (3)	3.1345 (18)	172 (3)
O3—H3*A*···Cl1^{viii}	0.82 (3)	2.36 (3)	3.1703 (19)	167 (3)
O2—H2*B*···Cl1^{ix}	0.89 (4)	2.31 (4)	3.1689 (18)	164 (3)
O2—H2*A*···Cl1^{i}	0.86 (4)	2.28 (4)	3.1369 (18)	172 (3)
O1—H1*B*···Cl1^{x}	0.81 (4)	2.35 (4)	3.1500 (18)	171 (4)
O1—H1*A*···Cl2^{xi}	0.75 (3)	2.44 (3)	3.1863 (19)	171 (3)
O3—H3*B*···Cl2^{vii}	0.81 (3)	2.34 (3)	3.1345 (18)	172 (3)
O3—H3*A*···Cl1^{viii}	0.82 (3)	2.36 (3)	3.1703 (19)	167 (3)
O2—H2*B*···Cl1^{ix}	0.89 (4)	2.31 (4)	3.1689 (18)	164 (3)
O2—H2*A*···Cl1^{i}	0.86 (4)	2.28 (4)	3.1369 (18)	172 (3)
O1—H1*B*···Cl1^{x}	0.81 (4)	2.35 (4)	3.1500 (18)	171 (4)
O1—H1*A*···Cl2^{xi}	0.75 (3)	2.44 (3)	3.1863 (19)	171 (3)
O3—H3*B*···Cl2^{vii}	0.81 (3)	2.34 (3)	3.1345 (18)	172 (3)
O3—H3*A*···Cl1^{viii}	0.82 (3)	2.36 (3)	3.1703 (19)	167 (3)
O2—H2*B*···Cl1^{ix}	0.89 (4)	2.31 (4)	3.1689 (18)	164 (3)
O2—H2*A*···Cl1^{i}	0.86 (4)	2.28 (4)	3.1369 (18)	172 (3)
O1—H1*B*···Cl1^{x}	0.81 (4)	2.35 (4)	3.1500 (18)	171 (4)
O1—H1*A*···Cl2^{xi}	0.75 (3)	2.44 (3)	3.1863 (19)	171 (3)
O3—H3*B*···Cl2^{vii}	0.81 (3)	2.34 (3)	3.1345 (18)	172 (3)
O3—H3*A*···Cl1^{viii}	0.82 (3)	2.36 (3)	3.1703 (19)	167 (3)
O2—H2*B*···Cl1^{ix}	0.89 (4)	2.31 (4)	3.1689 (18)	164 (3)
O2—H2*A*···Cl1^{i}	0.86 (4)	2.28 (4)	3.1369 (18)	172 (3)
O1—H1*B*···Cl1^{x}	0.81 (4)	2.35 (4)	3.1500 (18)	171 (4)
O1—H1*A*···Cl2^{xi}	0.75 (3)	2.44 (3)	3.1863 (19)	171 (3)
O1—H1*A*···Cl2^{xi}	0.75 (3)	2.44 (3)	3.1863 (19)	171 (3)
O1—H1*B*···Cl1^{x}	0.81 (4)	2.35 (4)	3.1500 (18)	171 (4)
O2—H2*A*···Cl1^{i}	0.86 (4)	2.28 (4)	3.1369 (18)	172 (3)
O2—H2*B*···Cl1^{ix}	0.89 (4)	2.31 (4)	3.1689 (18)	164 (3)
O3—H3*A*···Cl1^{viii}	0.82 (3)	2.36 (3)	3.1703 (19)	167 (3)
O3—H3*B*···Cl2^{vii}	0.81 (3)	2.34 (3)	3.1345 (18)	172 (3)

O1—H1*A*···Cl2^{xi}	0.75 (3)	2.44 (3)	3.1863 (19)	171 (3)
O1—H1*B*···Cl1^{x}	0.81 (4)	2.35 (4)	3.1500 (18)	171 (4)
O2—H2*A*···Cl1^{i}	0.86 (4)	2.28 (4)	3.1369 (18)	172 (3)
O2—H2*B*···Cl1^{ix}	0.89 (4)	2.31 (4)	3.1689 (18)	164 (3)
O3—H3*A*···Cl1^{viii}	0.82 (3)	2.36 (3)	3.1703 (19)	167 (3)
O3—H3*B*···Cl2^{vii}	0.81 (3)	2.34 (3)	3.1345 (18)	172 (3)
O1—H1*A*···Cl2^{xi}	0.75 (3)	2.44 (3)	3.1863 (19)	171 (3)
O1—H1*B*···Cl1^{x}	0.81 (4)	2.35 (4)	3.1500 (18)	171 (4)
O2—H2*A*···Cl1^{i}	0.86 (4)	2.28 (4)	3.1369 (18)	172 (3)
O2—H2*B*···Cl1^{ix}	0.89 (4)	2.31 (4)	3.1689 (18)	164 (3)
O3—H3*A*···Cl1^{viii}	0.82 (3)	2.36 (3)	3.1703 (19)	167 (3)
O3—H3*B*···Cl2^{vii}	0.81 (3)	2.34 (3)	3.1345 (18)	172 (3)
O1—H1*A*···Cl2^{xi}	0.75 (3)	2.44 (3)	3.1863 (19)	171 (3)
O1—H1*B*···Cl1^{x}	0.81 (4)	2.35 (4)	3.1500 (18)	171 (4)
O2—H2*A*···Cl1^{i}	0.86 (4)	2.28 (4)	3.1369 (18)	172 (3)
O2—H2*B*···Cl1^{ix}	0.89 (4)	2.31 (4)	3.1689 (18)	164 (3)
O3—H3*A*···Cl1^{viii}	0.82 (3)	2.36 (3)	3.1703 (19)	167 (3)
O3—H3*B*···Cl2^{vii}	0.81 (3)	2.34 (3)	3.1345 (18)	172 (3)

Symmetry codes: (i) *x*+1/2, *y*−1/2, *z*; (vii) −*x*+1, *y*−1, −*z*+1/2; (viii) −*x*+1, −*y*+1, −*z*+1; (ix) −*x*+1, *y*, −*z*+1/2; (x) *x*+1/2, −*y*+3/2, *z*+1/2; (xi) −*x*+1/2, *y*−1/2, −*z*+1/2.

Hydrogen-bond geometry (Å, °) for the monoclinic form of carnallite

D—H···*A*	D—H	H···*A*	D···*A*	D—H···*A*
O3—H3*B*···Cl2^{i}	0.86 (4)	2.29 (4)	3.134 (2)	169 (3)
O3—H3*A*···Cl1^{ii}	0.87 (4)	2.31 (4)	3.170 (2)	170 (4)
O2—H2*B*···Cl1^{iii}	0.97 (4)	2.24 (4)	3.169 (2)	161 (3)
O2—H2*A*···Cl1^{iv}	0.91 (5)	2.24 (5)	3.136 (2)	168 (4)
O1—H1*B*···Cl1^{v}	0.81 (5)	2.35 (5)	3.150 (2)	171 (4)
O1—H1*A*···Cl2^{vi}	0.85 (5)	2.34 (5)	3.184 (2)	169 (4)

Symmetry codes: (i) -*x*+1, *y*-1, -*z*+1/2; (ii) -*x*+1, -*y*+1, -*z*+1; (iii) -*x*+1, *y*, -*z*+1/2; (iv) *x*+1/2, *y*-1/2, *z*; (v) *x*+1/2, -*y*+3/2, *z*+1/2; (vi) -*x*+1/2, *y*-1/2, -*z*+1/2.